

Observational Analysis of Heavy Rainfall Mechanisms Associated with Severe Tropical Storm Bilis (2006) after Its Landfall

SHUANZHU GAO

China National Meteorological Center, Beijing, China

ZHIYONG MENG

Department of Atmospheric Sciences, School of Physics, Peking University, Beijing, China

FUQING ZHANG

Department of Meteorology, The Pennsylvania State University, University Park, Pennsylvania

LANCE F. BOSART

Department of Atmospheric Sciences, University at Albany, State University of New York, Albany, New York

(Manuscript received 5 June 2008, in final form 8 December 2008)

ABSTRACT

This observational study attempts to determine factors responsible for the distribution of precipitation over large areas of southern China induced by Bilis, a western North Pacific Ocean severe tropical storm that made landfall on the southeastern coast of mainland China on 14 July 2006 with a remnant circulation that persisted over land until after 17 July 2006. The heavy rainfalls associated with Bilis during and after its landfall can be divided into three stages. The first stage of the rainfall, which occurred in Fujian and Zhejiang Provinces, could be directly induced by the inner-core storm circulation during its landfall. The third stage of rainfall, which occurred along the coastal areas of Guangdong and Fujian Provinces, likely resulted from the interaction between Bilis and the South China Sea monsoon enhanced by topographical lifting along the coast. The second stage of the rainfall, which appeared inland around the border regions between Jiangxi, Hunan, and Guangdong Provinces, caused the most catastrophic flooding and is the primary focus of the current study. It is found that during the second stage of the rainfall all three ingredients of deep moist convection (moisture, instability, and lifting) are in place. Several mechanisms, including vertical wind shear, warm-air advection, frontogenesis, and topography, may have contributed simultaneously to the lifting necessary for the generation of the heavy rainfall at this stage.

1. Introduction

Freshwater flooding associated with landfalling tropical cyclones (TCs) is one of the major threats to both life and property along coastal regions of the world. It accounted for about 60% of the total fatalities caused by TCs in the United States during 1970–99 (Rappaport 2000). Despite a steady increase in the skill of predicting tracks in recent years, there has been little progress in

forecasting TC intensity and rainbands (Pasch et al. 2004; Beven and Franklin. 2004; Houze et al. 2007). Rainfalls induced by TCs are often multiscale in nature, with their magnitude and distribution affected by many factors such as storm size, morphology, track, translation speed, cold-air damming, and the TC's interaction with synoptic and mesoscale features such as vertical wind shear, upper-level trough, and/or surface frontal boundaries. A precipitation forecast of a landfalling TC is further complicated by the coastal and inland topography as well as by land surface and boundary layer conditions (Lin et al. 2001b; Li et al. 2003).

Many previous studies on the distribution of TC-associated convection focus primarily on extratropical

Corresponding author address: Dr. Zhiyong Meng, Department of Atmospheric Sciences, School of Physics, Peking University, Beijing, China.
E-mail: zymeng@pku.edu.cn

transition (Atallah and Bosart 2003; Atallah et al. 2007), impact of boundary layer friction (Shapiro 1983), and vertical wind shear (Willoughby et al. 1984; Jones 1995, 2000a,b; Bender 1997; Frank and Ritchie 1999, 2001; Corbosiero and Molinari 2002, 2003; Rogers et al. 2003; Braun et al. 2006; Chen et al. 2006; Cecil 2007; Braun and Wu 2007). Zhao et al. (2005) found that a low-level cyclonic circulation and subsequent uplifting by an upper-level potential vorticity (PV) anomaly were primarily responsible for the torrential rainfall over inland China caused by Typhoon 9907 during its extratropical transition. In examining rainfall mechanisms associated with the extratropical transition of Hurricane Floyd (1999), Colle (2003) showed that a combination of strong frontogenesis, moist symmetric instability below 800 hPa, and slantwise neutrality aloft caused a narrow and intense rainband just inland of the coast.

Rainfall associated with a TC can become asymmetric after its landfall. The asymmetry of the TC rainfall can be attributed partly to the impact of the storm translation. Maximum convergence was found in the forward flank and to the right of a translating vortex due to asymmetric friction in the boundary layer (Shapiro 1983; Bender 1997; Frank and Ritchie 1999; Lonfat et al. 2004).

Vertical wind shear is another factor that could make the rainfall around a TC highly asymmetric. Corbosiero and Molinari (2003) speculated that the impact of storm motion on the distribution of its associated convection could be just a reflection of vertical wind shear. Hypotheses about the impact of vertical shear on the rainfall distribution have been put forward through numerical studies. Under an adiabatic condition, vertical wind shear may tilt the vortex and place the maximum rainfall on the right side of the tilt vector (Jones 1995; Frank and Ritchie 2001). Latent heat release in diabatic environment could change this relationship. In that situation, the relative inflow mechanism, which attributes the vertical motion to low-level convergence and upper-level divergence required to balance the low-level negative vorticity advection and the upper-level divergence by the relative flow on the downshear side, has been put forward (Wang and Holland 1996; Bender 1997; Frank and Ritchie 2001; Braun et al. 2006; Wu et al. 2006). Advected by the TC's cyclonic circulation, the rainfall may also appear on the downshear left (Frank and Ritchie 2001). The juxtaposition between vertical shear and convection signatures was also examined through observational studies using radar reflectivity (Willoughby et al. 1984), rainfall (Chen et al. 2006), lightning (Corbosiero and Molinari 2002, 2003) and satellite-derived rain rate (Cecil 2007). These studies showed that the asymmetric pattern of rainfall was closely related to the storm strength, the magnitude

of vertical shear, and the distance of rainfall to the storm center. It was found that TC inner-core rainfall (within radii of 100 km from the storm center) preferentially occurred at a location on the downshear left and that the outer rainband (beyond radii of 400 km) tended to be located on the downshear right (Corbosiero and Molinari 2002; Cecil 2007). In addition, a loosely organized TC tended to have maximum rainfall on the downshear right.

Topography is another important factor that could contribute to the asymmetry of landfalling TC rainfall. The moist air forced up the slope of coastal hills and mountain chains can lead to much heavier rainfall than that over flat terrain. Lin et al. (2001a) put forward the idea that topographic rainfall could be contributed by a combination of common ingredients such as the presence of a moist, moderate-to-intense low-level jet; an unstable, high moist, and confluent upstream airflow; steep topography; favorable mountain geometry; strong environmentally forced upward motion; and a preexisting slow-moving large-scale convective system. Several cases of severe flooding caused by landfalling TCs in China were found to be closely related to topography, such as the torrential rainfall to the east of the Funiu Mountain in Henan Province in August of 1975 with a 24-h rainfall of 1060 mm (Li et al. 2003).

In July of 2006, Bilis, a severe tropical storm (surface sustained maximum wind speed between 24.5 and 32.6 m s⁻¹) in the western North Pacific Ocean, made landfall on the coast of Fujian Province, China. Bilis was not particularly intense at landfall and further weakened gradually thereafter. Its track was well predicted by the China National Meteorological Center (CNMC), but the real-time forecast greatly underestimated the intensity of the heavy rainfall, which triggered large-area severe flooding after the storm moved inland.

The current study seeks to investigate possible mechanisms of the heavy rainfall associated with Bilis. Section 2 introduces the data used in this study. A brief synoptic overview of Bilis is given in section 3. Section 4 describes a three-stage evolution of the rainfall associated with Bilis. Dynamical processes that lead to the second stage of the rainfall are examined in section 5. A summary and discussion are given in section 6.

2. Data

The data used for this study include the final (FNL) analyses of the Global Forecasting System of the National Centers for Environmental Prediction (NCEP); conventional surface, radiosonde, and satellite observations; and hourly rainfall observations from the surface mesoscale observing network of China provided by the real-time dataset of CNMC. The FNL data have a

horizontal resolution of $1^\circ \times 1^\circ$ longitude and latitude and include the surface level and 26 mandatory pressure levels (i.e., 1000, 975, 950, 925, 900, 850, 800, 750, 700, 650, 600, 550, 500, 450, 400, 350, 300, 250, 200, 150, 100, 70, 50, 30, 20, and 10 hPa). All figures were created using the FNL gridded analysis except where otherwise specified. The best track and intensity data of Bilis were provided by the Shanghai Typhoon Institute of China.

3. Overview of Bilis

Bilis formed about 1100 km to the east of the southern Philippines on 9 July 2006. It became a severe tropical storm (surface maximum sustained wind speed of $24.5\text{--}32.6\text{ m s}^{-1}$, from the international TC categorization) at 0000 UTC 11 July while it was moving northwestward at a speed of $15\text{--}20\text{ km h}^{-1}$. It made its first landfall on Taiwan at 1500 UTC 13 July with a maximum sustained wind speed of 30 m s^{-1} , which is just shy of the 32.7 m s^{-1} intensity needed to be categorized as a typhoon (Fig. 1). Bilis entered the Taiwan Strait at 1900 UTC 13 July and subsequently made its second landfall in the Xiapu county of Fujian Province around 0500 UTC 14 July, also with a maximum sustained wind speed of 30 m s^{-1} . Bilis was downgraded to a tropical storm (surface sustained maximum wind speed between 17.2 and 24.4 m s^{-1}) in the Minhou county of Fujian Province shortly after its second landfall while it was moving westward at $10\text{--}15\text{ km h}^{-1}$. Bilis further weakened into a tropical depression (surface maximum sustained wind speed of less than 17.1 m s^{-1}) at 0700 UTC 15 July in Jiangxi Province and continued moving westward and later west-southwestward. The remnant of the Bilis depression moved into Vietnam and dissipated there on 17 July.

Using the online dataset (<http://www.cdc.noaa.gov/>) maintained by the National Oceanic and Atmospheric Administration Earth System Research Laboratory, we analyzed the mean geopotential height for the period from 0600 UTC 13 July to 0600 UTC 16 July 2006 at 300 hPa (solid contours in Fig. 2a). The result shows that a broad, strong anticyclone is persistent over middle to north China. This strong anticyclone blocks Bilis from moving northward. At 500 hPa, the subtropical high over the western North Pacific intensifies and expands westward into China and subsequently forms an east-west-oriented high pressure belt in the mid- to upper troposphere to the north of Bilis, which further steers the storm moving northwestward to westward and later to west-southwestward (Fig. 3). The westward extension of the 500-hPa height contours of 5840, 5860, and 5880 gpm is apparent from 0000 UTC 14 July to 0000 UTC 15 July 2006. The subtropical high splits at around 1200 UTC 15 July 2006. From then on, Bilis has been steered

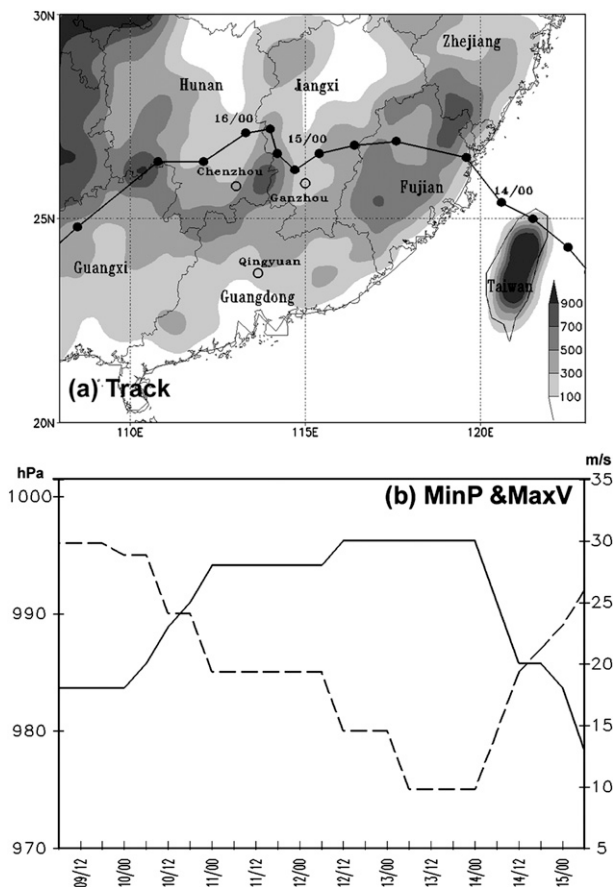


FIG. 1. (a) The best track of Bilis with positions plotted every 6 h. Also plotted are terrain heights (shaded every 200 m). The names of related provinces have been labeled. The names of the three radiosonde stations (marked as open circles) to be plotted in Fig. 4 are also labeled here. (b) Intensity evolution of Bilis in terms of minimum sea level pressure (dashed) and maximum surface wind (solid).

southwestward by the western part of the split subtropical high.

At 850 hPa, the 3-day-averaged geopotential height shows a low system expanding much of central and eastern China during this event (shaded in Fig. 2a). The low at 850 hPa in conjunction with the high 300-hPa height indicates deep warm air over this region. The potential temperature at 850 hPa (thin contours in Fig. 3) over inland China is higher than that over the open ocean indicating a moderately strong, quasi-stationary frontal zone along the east coast of China that gradually retreats inland after the arrival of Bilis.

There is also abundant moisture over a large area of southern and central China during the life cycle of Bilis. The strong southerly-to-southwesterly flow at 850 hPa over the southeastern coast of China between 20° and 30°N indicates that the monsoon is strong, which acts

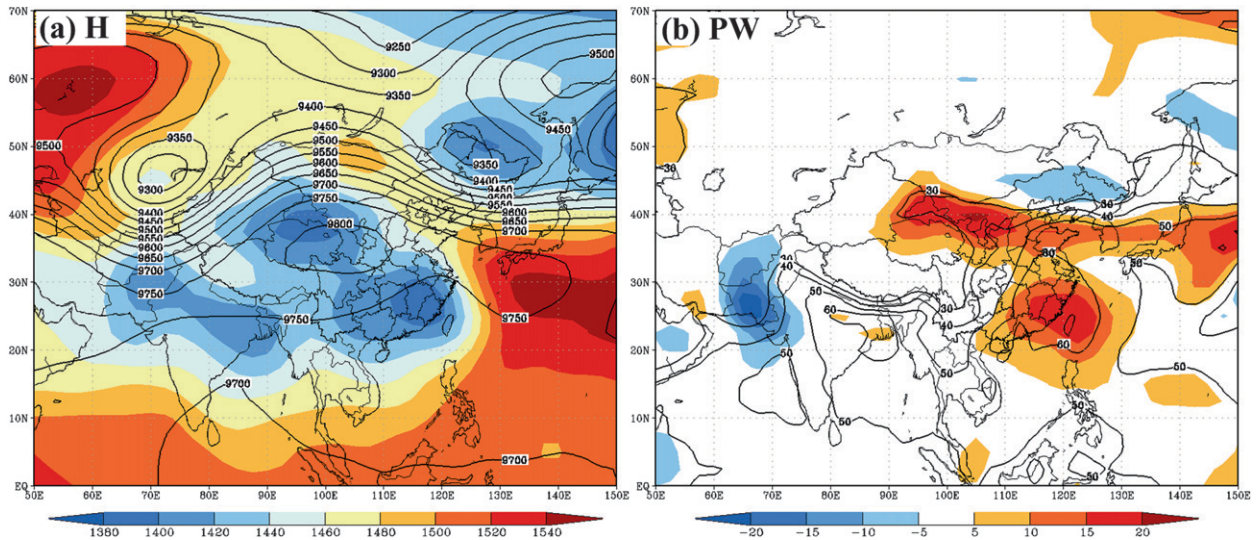


FIG. 2. (a) The mean geopotential height at 300 hPa (contoured every 50 gpm) and 850 hPa (shaded every 20 gpm) averaged over 0600 UTC 13 Jul–0600 UTC 16 Jul 2006. (b) The column-integrated precipitable water (contoured every 10 kg m⁻² starting from 30 kg m⁻²) averaged over 0600 UTC 13 Jul–0600 UTC 16 Jul 2006 and its anomaly from the 1968–96 climatological mean (shaded every 5 kg m⁻²).

as an important source of moisture (Fig. 2a). As a result, the event-averaged column-integrated precipitable water in southeast China averaged over 0600 UTC 13 July–0600 UTC 16 July 2006 is generally larger than 60 kg m⁻² with a maximum well over 65 kg m⁻² (contour in Fig. 2b), which is considerably higher than its climate average during 1968–96 (shaded in Fig. 2b). The instantaneous values are even higher (Fig. 3). For example, at 0000 UTC 15 July, the column-integrated precipitable water reaches 79.4 kg m⁻² at Ganzhou in Jiangxi Province (Figs. 3c and 4b).

Bilis produced extensive precipitation over land with event-total accumulated rainfall of more than 100 mm covering most parts of south China (shaded in Fig. 5a). The heavy rainfall caused severe flooding that affected six provinces, including Fujian, Zhejiang, Jiangxi, Hunan, Guangdong, and Guangxi Provinces. At least 843 people were reportedly killed (a new 10-yr record of TC associated fatalities in China; China Meteorological Administration 2007). More than 3 million people were evacuated. The direct economic loss reached 35 billion RMB (or approximately US\$5 billion).

4. The three-stage rainfall evolution over land

Bilis differs from many other catastrophic rainfall events associated with landfalling TCs over mainland China in that these storms usually move north or northwestward while interacting with a midlatitude baroclinic system to the north (e.g., Duan 2006), whereas Bilis was forced to move slowly west and southwestward. As a result, large moisture was maintained over south China

(Fig. 3, shaded), which helped to sustain heavy, persistent rainfall over this region.

As shown in the accumulated rainfall of Fig. 5 and the satellite images of Fig. 6, the inland rainfall associated with Bilis is most pronounced to the left (south) side of its track, but the rainfall intensity and distribution varies notably with time. To better explore possible contributors to the distribution of rainfall associated with Bilis at different times, the observed rainfall over land associated with Bilis is grouped into three stages based on the timing and location of their occurrence (Fig. 5).

The first stage of the rainfall is defined for the rainfall appearing at the coastal area of Fujian and Zhejiang Provinces between 1200 UTC 13 July and 1200 UTC 14 July (Fig. 5b) right before and after Bilis's second landfall. As a result of the inner-core circulation and the outer rainbands interacting with the coastal terrains, heavy rainfall began to fall at approximately 1200 UTC 13 July in the coastal area of northern Fujian Province and southern Zhejiang Province and later expanded to most part of Jiangxi and Fujian Provinces. During this stage, rainfall was generally within about 300 km of the storm center in all quarters but with the prevalence to the forward right (Figs. 5b and 6a). This right-front quadrant location of the maximum rainfall during the TC landfall in the Northern Hemisphere has been demonstrated in both observational (Cline 1926; Miller 1964; Powell 1987) and numerical studies (Tuleya and Kurihala 1978; Jones 1987) and is likely due to the frictional convergence induced by the differential friction between land and sea (Dunn and Miller 1960). The

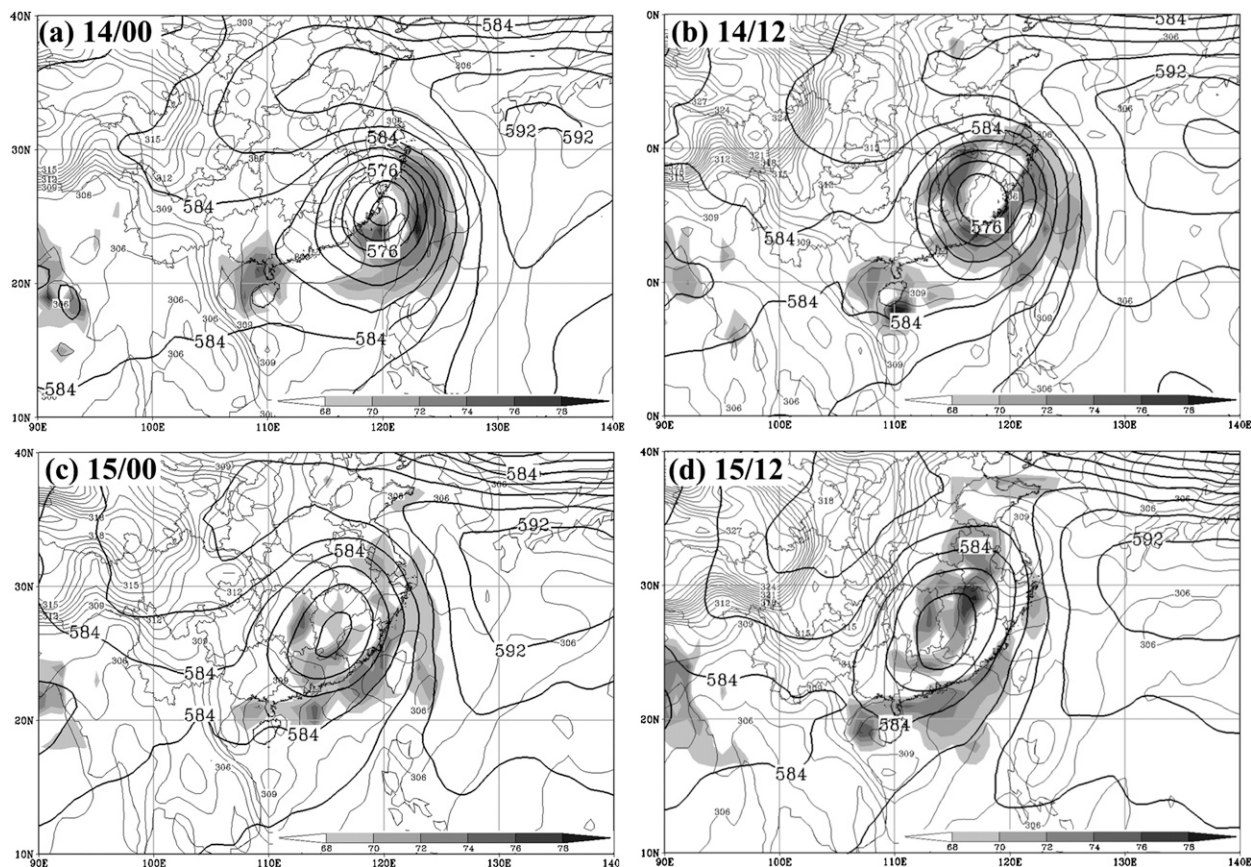


FIG. 3. Geopotential height at 500 hPa (gpm/10), column-integrated precipitable water (shaded every 2 kg m^{-2}), and potential temperature (thin contours every 1 K) at 850 hPa for (a) 0000 UTC 14 Jul, (b) 1200 UTC 14 Jul, (c) 0000 UTC 15 Jul, and (d) 1200 UTC 15 Jul 2006.

magnitude of precipitation decreased gradually from the coastal area toward inland, coinciding with the weakening of Bilis. During this stage, the precipitation in the coastal areas of southern Zhejiang and northern Fujian Provinces was generally greater than 100 mm while in Jiangxi Province only 25–50 mm of rainfall were observed. This stage of rainfall was generally well predicted by the official forecast of CNMC (contours in Fig. 5b).

The second stage of rainfall is defined for the rainfall observed from approximately 0600 UTC 14 July until approximately 1800 UTC 15 July along the border regions between Jiangxi, Hunan, and Guangdong Provinces. The rainfall between 1200 UTC 14 July and 1200 UTC 15 July, the most intense precipitation during this stage, is plotted in Fig. 5c. The rainfall for this stage was apparently separated from the first stage, which can also be observed from satellite images (e.g., at 1200 and 1800 UTC 14 July in Figs. 6b,c). With a westward movement of the weakened TC and the gradual dissipation of the intense inner core, the cloud and rainfall patterns be-

came more and more widespread and asymmetric, with a significant enhancement to the west and south (forward and left) of the TC. The 24-h accumulated rainfall valid at 1200 UTC 15 July was greater than 100 mm in northern Guangdong, southern Jiangxi, and southern Hunan Provinces with a localized maximum of greater than 250 mm recorded in Hunan Province. A large area of intensive rainfall in this area persisted until 1200 UTC 15 July, with lingering moderate rainfall in Hunan and Guangdong Provinces thereafter (Fig. 5d).

The 24-h official rainfall forecast issued by CNMC for the period between 1200 UTC 13 July and 1200 UTC 14 July 2006 (Fig. 5b) nearly completely missed the moderate rainfall observed between Hunan and Jiangxi Provinces. A subsequent 24-h forecast for the period between 1200 UTC 14 July and 1200 UTC 15 July 2006 was apparently improved but still underpredicted (Fig. 5c) the observed rainfall along the border regions between Hunan, Jiangxi, and Guangdong Provinces. It will be of both operational and research interest to understand the heavy rainfall mechanisms for this stage that caused

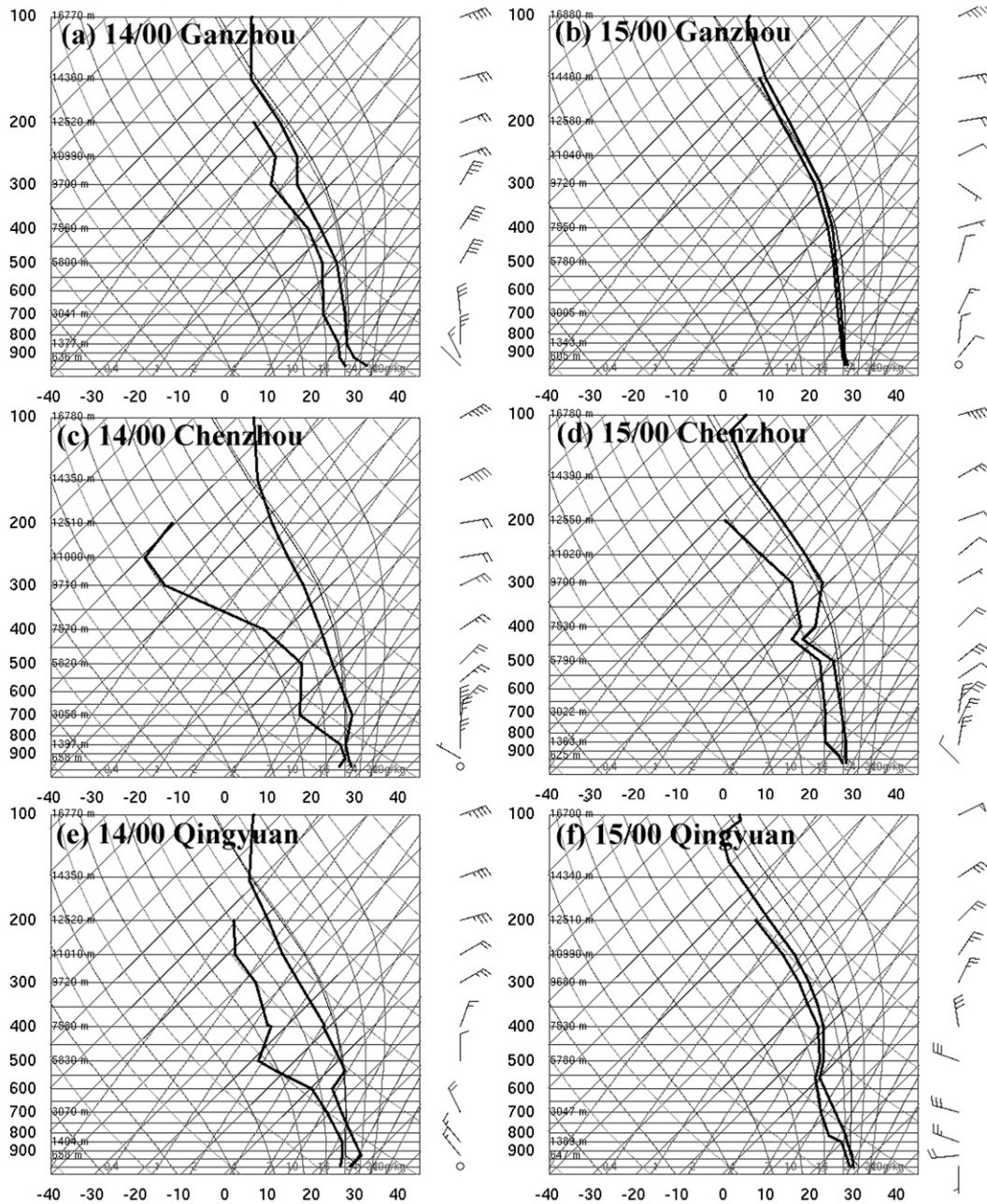


FIG. 4. Radiosondes of (a) Ganzhou at 0000 UTC 14 Jul 2006, (b) Ganzhou at 0000 UTC 15 Jul 2006, (c) Chenzhou at 0000 UTC 14 Jul 2006, (d) Chenzhou at 0000 UTC 15 Jul 2006, (e) Qingyuan at 0000 UTC 14 Jul 2006, and (f) Qingyuan at 0000 UTC 15 Jul 2006. These figures were derived from the University of Wyoming Web site. Locations of these stations are labeled in Fig. 1a. A full wind barb on the right of (a)–(f) represents 5 m s^{-1} .

widespread catastrophic flooding and subsequent large loss of life and property.

Because the majority of the rainfall during the second stage occurred over mountainous regions (Fig. 1a), it is widely suspected that the Nanling Mountains, the mountain range between Hunan and Guangdong Provinces, and its interaction with the TC circulation could be

important contributors to the excessive rainfall. In the meantime, the infrared satellite images from 1200 UTC 14 July to 1800 UTC 14 July 2006 (Figs. 6b,c) show that the convection associated with this stage of rainfall is localized. The next section will demonstrate that the three ingredients of deep moist convection are all in place during this stage of rainfall. Widespread moist and

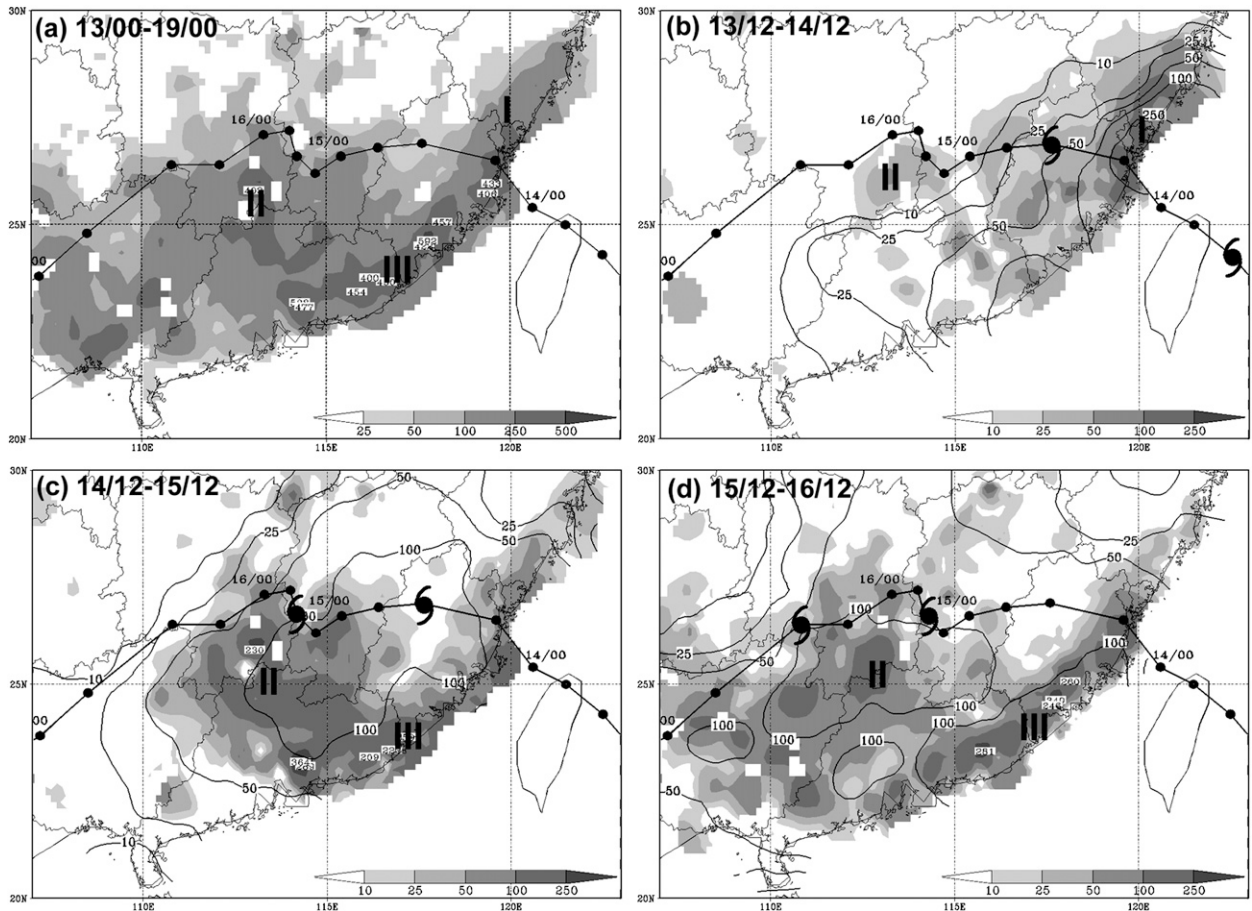


FIG. 5. Observed rainfall (shaded; mm) of Bilis during (a) 0000 UTC 13 Jul–0000 UTC 19 Jul, (b) 1200 UTC 13 Jul–1200 UTC 14 Jul, (c) 1200 UTC 14 Jul–1200 UTC 15 Jul, and (d) 1200 UTC 15 Jul–1200 UTC 16 Jul 2006. The “I,” “II,” and “III” labels denote the general locations of the three stages of the rainfall. The best track of Bilis is shown for reference in 6-h intervals. Locations of storm centers at the starting and ending times for the three stages are marked by typhoon symbols. The 24-h rainfall forecast issued by CNMC for the period ending at 1200 UTC 14 Jul, 1200 UTC 15 Jul, and 1200 UTC 16 Jul are also plotted for comparison in (b), (c), and (d), respectively, with the same scale as the observation.

unstable flow is observed. Several processes are likely contributing to lifting, such as vertical wind shear, warm-air advection, frontogenesis, and/or topographic forcing.

The third stage of the rainfall is defined for the rainfall occurring along the coastal areas of Guangdong and Fujian Provinces during 0600 UTC 15 July–1200 UTC 16 July starting before the end of the second stage of the rainfall. The most intense precipitation during this stage fell between 1200 UTC 15 July and 1200 UTC 16 July as plotted in Fig. 5d. The strong southwesterly flow brought abundant moisture from the South China Sea to the rainfall area (Fig. 3d). The heavy-precipitation belt (>100 mm) extended 100 km inland from the coast, spanning nearly 700 km in length with the maximum rainfall rate at around 1800 UTC 15 July. Operational forecasting for this stage of rainfall was very successful (Fig. 5d). This stage of rainfall was likely caused by the

interaction of the much-weakened Bilis circulation with the South China Sea monsoon along with lifting by the coastal topography.

5. Mechanisms of the second stage of the rainfall

Satellite imageries of Bilis in the second stage of rainfall show that the rainfall is localized with areas of bright, white cloud tops indicating occurrence of convective rainfall (Fig. 6). This section examines each of the three ingredients for deep moist convection: moisture, instability, and lifting (e.g., Doswell et al. 1996). First, rich moisture was observed throughout the life span of Bilis (Fig. 2b), with high precipitable water in southern Jiangxi, Hunan, and northern Guangdong Provinces (Figs. 3b,c). Second, the instability condition was found favorable for moist convection. The large convective available potential energy

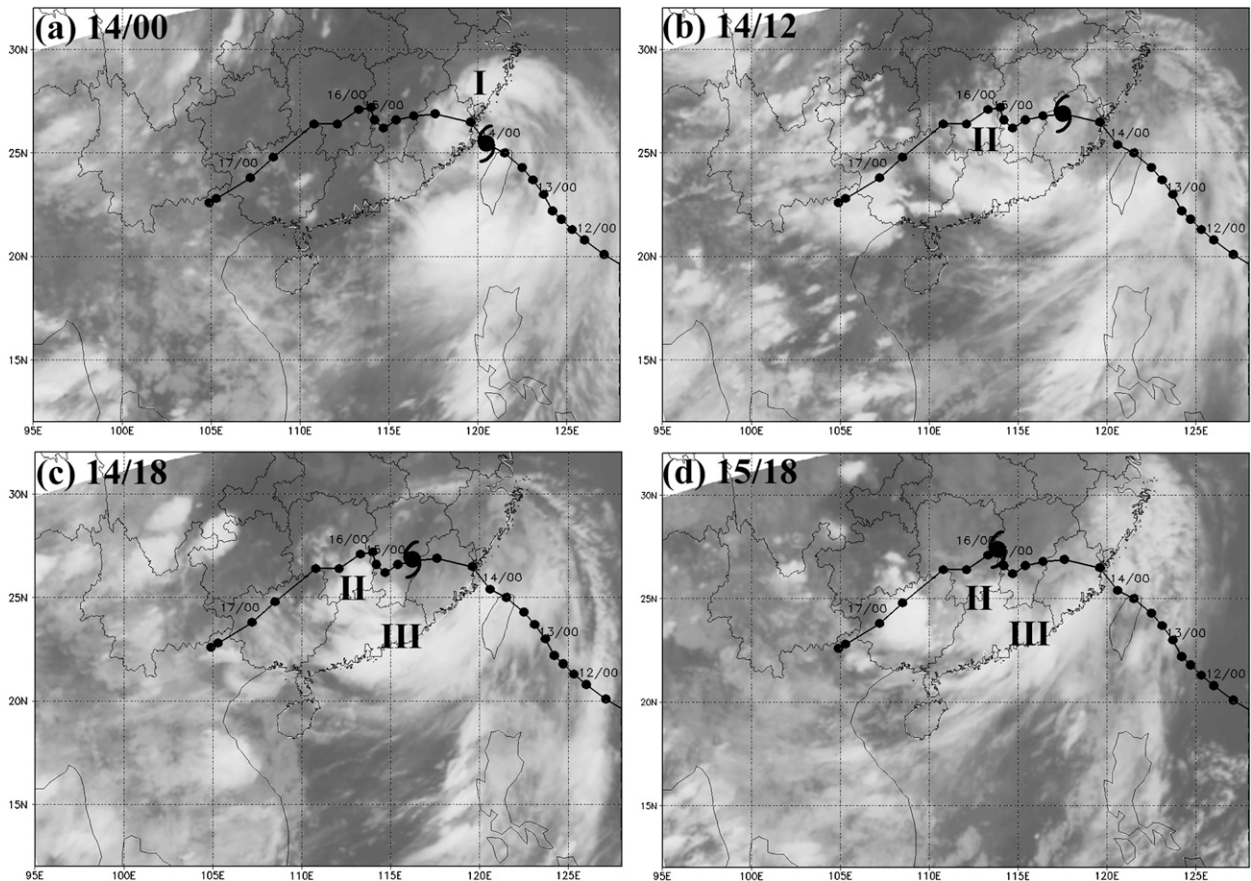


FIG. 6. Infrared satellite imageries at (a) 0000 UTC 14 Jul, (b) 1200 UTC 14 Jul, (c) 1800 UTC 14 Jul, and (d) 1800 UTC 15 Jul 2006. The “I,” “II,” and “III” labels denote the general locations of the three stages of rainfall. The TC center at the labeled time is marked by typhoon symbols. The track of Bilis is also given for reference.

(CAPE) area with its magnitude of more than 1000 J kg^{-1} shifted gradually from Jiangxi to Hunan and then to Guangxi Provinces. However, the heavy rainfall was observed on the edge of the maximum center (Figs. 7a,b), likely because of the effect of existing precipitation. On the other hand, the vertical gradient of saturation equivalent potential temperature θ_{es} , which is an index for conditional instability, correlates well with the heavy rainfall in this stage. The overlapping area between where θ_{es} decreases with height (shaded in Figs. 7c,d) and lifting is well consistent with location of heavy rainfall. This result suggests that strong conditional instability was in place for the occurrence of deep moist convection in the second stage of rainfall. Besides moisture and instability, mechanisms contributing to lifting, which is another ingredient of deep moist convection, will be addressed next.

a. Impact of topography

As shown in Fig. 1, the concave-shaped Nanling Mountain Range is located along the border between Jiangxi, Hunan, and Guangdong Provinces. It covers an

area of about 300 km^2 and has more than 30 peaks, with their altitudes being between 800 and 1902 m. Previous studies showed that the Nanling Mountains could considerably enhance the rainfall associated with approaching TCs (Lin et al. 2001b; Li et al. 2004). When Bilis was approaching the Nanling Mountains, the northerly flow on the west side of Bilis was directed almost perpendicular to the main axis of the mountain range. This favorable topographic lifting applied on the high moist and unstable upstream airflow associated with this slow-moving TC [a combination of several ingredients for topographic precipitation as summarized by Lin et al. (2001a)] could have had a substantial impact on the rainfall in southeastern Hunan Province.

To explore further the impact of the Nanling Mountains on the rainfall, two numerical experiments were performed using the Advanced Research version of the Weather Research and Forecasting Model (WRF2.2). Three domains with two-way nesting were used (Fig. 8a). Domain 1 and domain 2 were started from 0000 UTC 14 Jul 2006, and domain 3 was started 6 h into the

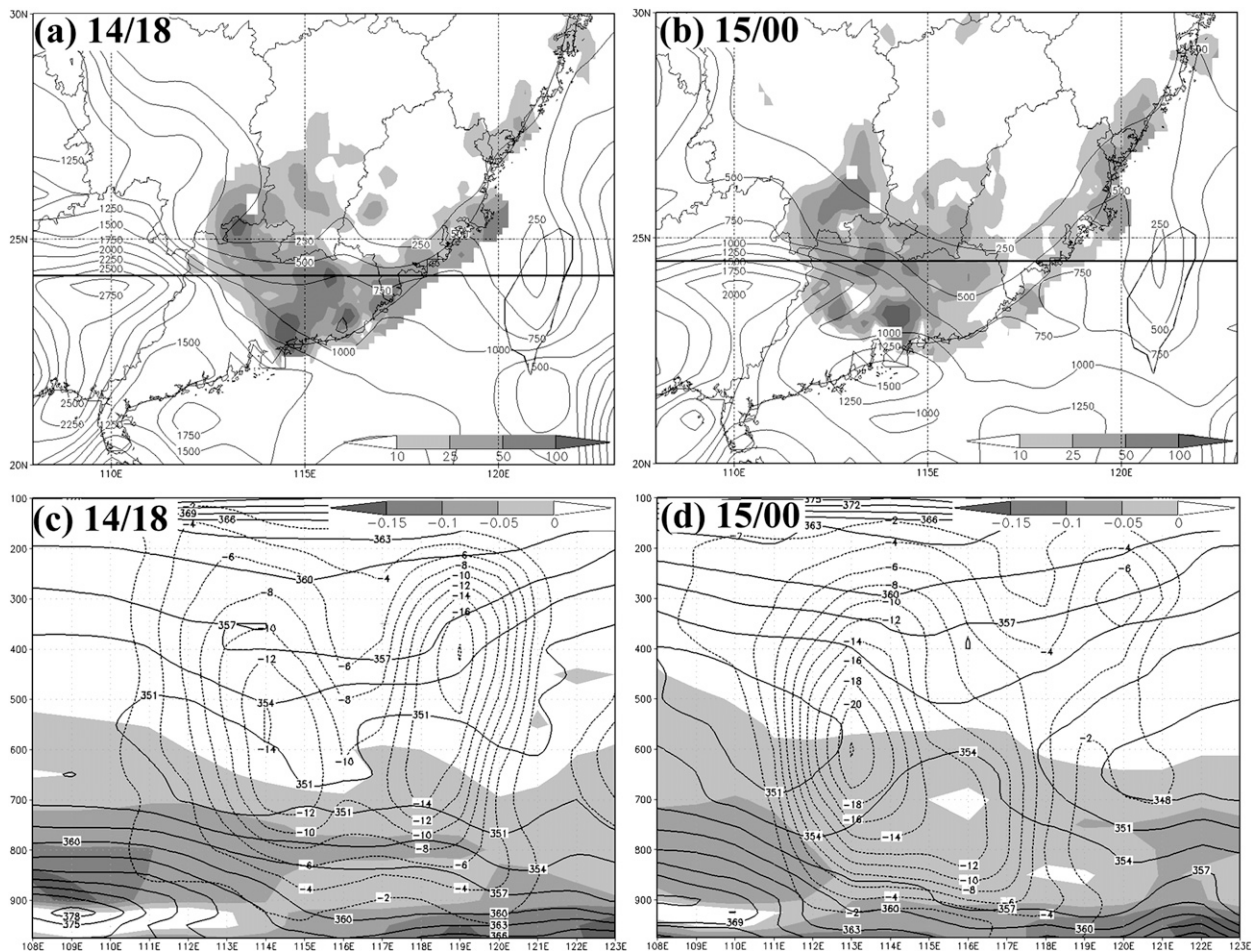


FIG. 7. CAPE (thin solid contours; J kg^{-1}) at (a) 1800 UTC 14 Jul and (b) 0000 UTC 15 Jul 2006 with 6-h rainfall (shaded) ± 3 h relative to the respective times. Also plotted are the vertical cross sections of saturation equivalent potential temperature (solid; K), negative changes of saturation equivalent potential temperature with height (shaded; K hPa^{-1}), and vertical velocity (dashed; $10^{-1} \text{ Pa s}^{-1}$) along the latitude of (c) 24.2°N at 1800 UTC 14 Jul 2006 and (d) 24.5°N at 0000 UTC 15 Jul 2006.

integration. All three domains were ended at 1200 UTC 15 July 2006. Domain 1 covered eastern Asia and most parts of the western North Pacific. Domain 2 covers the northwestern Pacific and most parts of China. Domain 3 covered southeastern China. Grid sizes of the coarse domain and the two inner domains were respectively 40.5, 13.5, and 4.5 km. All domains had 35 levels in vertical direction. Physical parameterization schemes included the Grell–Devenyi cumulus scheme (Grell and Devenyi 2002; for domains 1 and 2 only), WRF single-moment 6-class microphysics with graupel (Hong et al. 2004), and the Yonsei State University scheme (Noh et al. 2003) for planetary boundary layer processes. The FNL analyses were used to create the initial and boundary conditions. The WRF three-dimensional variational data assimilation was used to assimilate conventional sounding and surface observations covered by domain 1 into its initial field.

Two experiments were carried out as follows: 1) “CTL” is the control experiment in which the original terrain (shaded in Fig. 8b) was used and 2) “NoTer” is the experiment in which the terrain in southeastern China was reduced to 100 m (solid contours in Fig. 8b) wherever the terrain is above 100 m. In CTL, the simulated track (solid line marked with empty circles) is close to the best track (solid line marked with filled circles). The 36-h track forecast error is only 50 km. The simulated 24-h rainfall between 1200 UTC 14 July and 1200 UTC 15 July 2006 (Fig. 8c) captures both the general pattern and the details of the observed rainfall (Fig. 5c), especially the rainfall in southern Hunan Province. Decreasing the height of the topography only has a minor impact on the simulated track (dashed line marked with empty circles in Fig. 8b). The patterns of 24-h rainfall during 1200 UTC 14 July–1200 UTC 15 July 2006 in CTL and NoTer are also similar except for

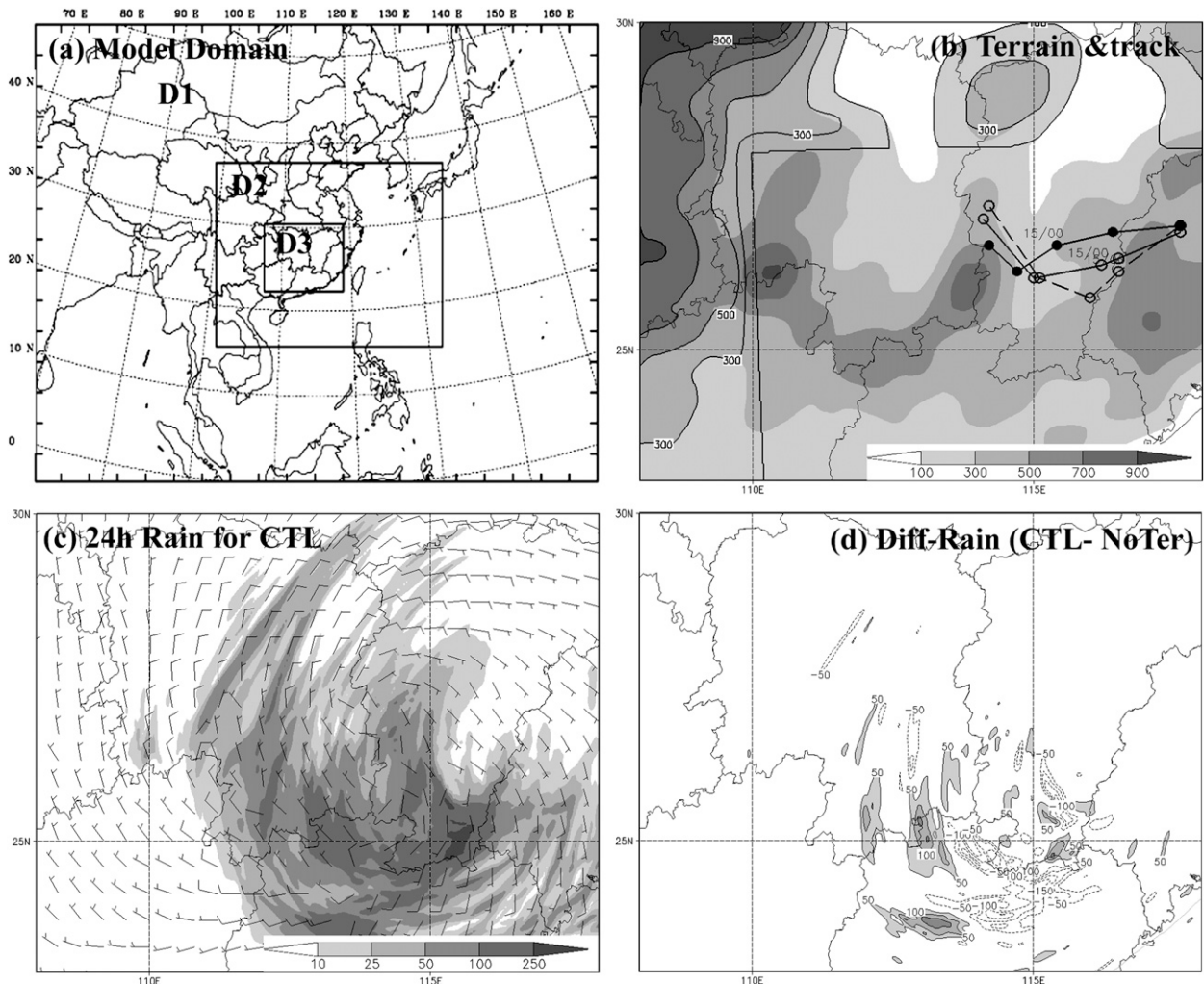


FIG. 8. The impact of topography on the second stage of rainfall examined by numerical experiment. (a) The model domains. (b) The topography for control experiment “CTL” (shaded contours every 200 m) and sensitivity experiment “NoTer” (solid contours every 200 m) in which the terrain in southeastern China that is above 100 m is reduced to 100 m. The best track of Bilis (solid line marked by solid circles), the simulated track in CTL (solid line marked by open circles), and the simulated track in NoTer (dashed line marked by open circles) are plotted. (c) The 24-h simulated rainfall (mm) in CTL between 1200 UTC 14 Jul and 1200 UTC 15 Jul 2006. The wind vector (full barb = 10 m s^{-1}) is 10-m wind at 1200 UTC 15 Jul 2006. (d) The difference of the 24-h simulated rainfall between CTL and NoTer (contours every 50 mm; areas with differences larger than 50 mm are shaded).

the rainfall in southern Hunan and northern Guangdong Provinces (Fig. 8d). Without the high terrain of the Nanling Mountains, the rainfall in the southern tip of Hunan Province decreases considerably. In the meantime, more rainfall appears downstream in Guangdong Province without the blocking of the Nanling Mountains. This result shows that topographic lifting could have played a key role in the rainfall in southern Hunan Province. However, the main part of rainfall located in northern Guangdong and southern Jiangxi Provinces seems to be not closely related to topography. Their lifting mechanisms will be further examined.

b. Vortex–shear interaction

As mentioned in the introduction, many previous studies revealed that vertical wind shear is an important factor that could result in asymmetric TC-associated rainfall. The radiosondes of Ganzhou, Chenzhou, and Qingyuan at 0000 UTC 14 July and 0000 UTC 15 July (Fig. 4) show consistent southwestward vertical wind shear in southeastern China in the second stage of rainfall. To explore the impact of environmental vertical wind shear on the rainfall of this stage, the environmental vertical shear for Bilis was calculated in a

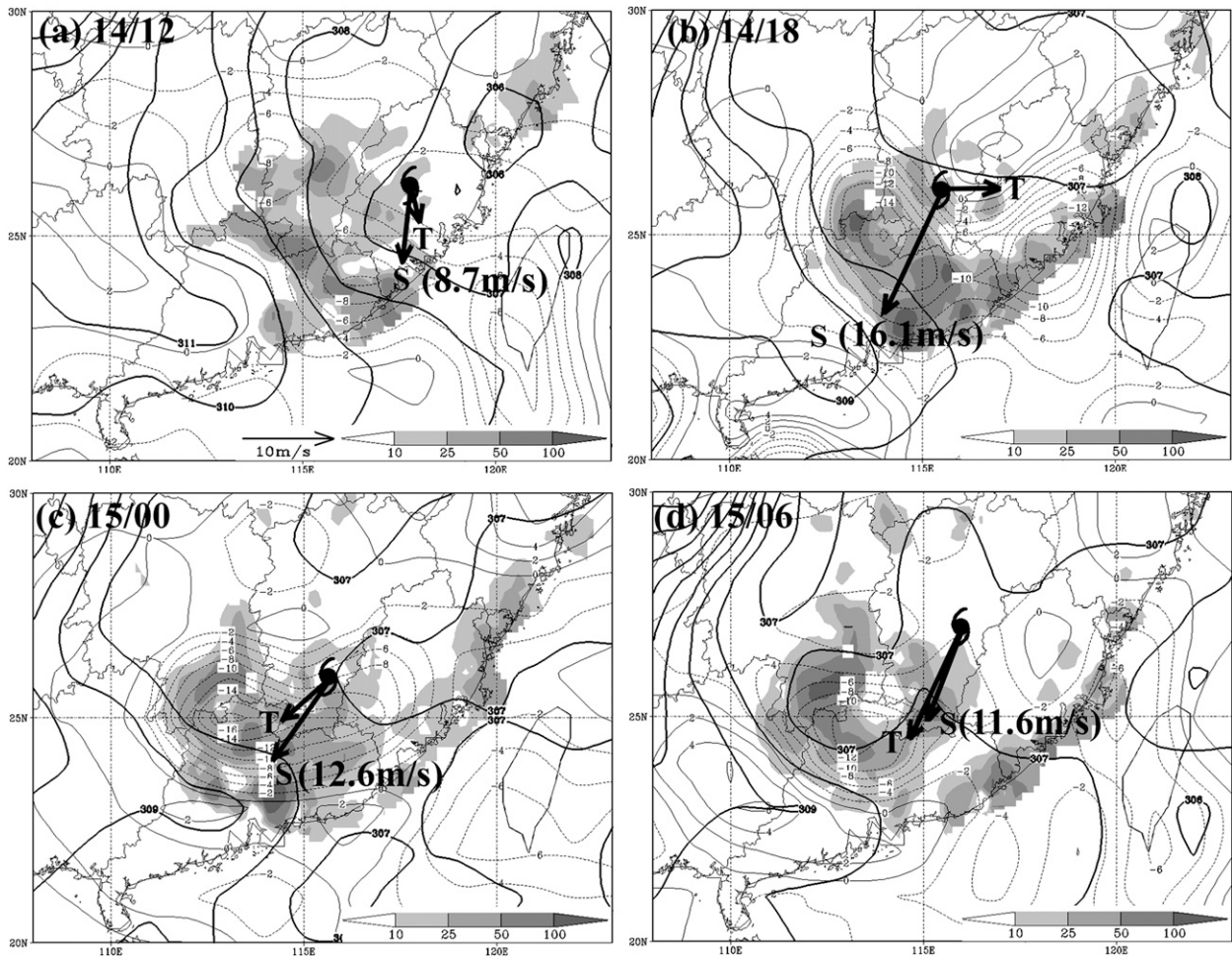


FIG. 9. Vertical wind shear (black arrow denoted by “S”) between 200 and 850 hPa and vortex-tilting vector (black arrow denoted by “T,” denoting a vector pointing from the vortex center at 850 hPa to that at 300 hPa) at (a) 1200 UTC 14 Jul, (b) 1800 UTC 14 Jul, (c) 0000 UTC 15 Jul, and (d) 0600 UTC 15 Jul 2006 with 6-h rainfall (shaded) ± 3 h relative to the respective times. The potential temperature (heavy contours every 1 K) at 850 hPa and the vertical velocity at 700 hPa (thin contours; $10^{-1} \text{ Pa s}^{-1}$) at the respective times are also plotted. The typhoon symbol denotes the circulation center of Bilis in the FNL analysis at 850 hPa at the corresponding times.

way similar to previous work (Chen et al. 2006; Cecil 2007) using the mean wind difference between 200 and 850 hPa averaged over a 200–800-km annulus from the storm center (vectors marked with “S” in Fig. 9; similar to the averages over a disk within 800 km—not shown). With the dominance of the subtropical high in the upper troposphere to the north (Fig. 2), the wind shear vectors are largely pointing toward the southwest and are 8.7, 16.1, 12.6, and 11.6 m s^{-1} for 1200 UTC 14 July, 1800 UTC 14 July, 0000 UTC 15 July, and 0600 UTC 15 July, respectively (Fig. 9). These large values of vertical wind shear may have larger impact than the storm motion (Corbosiero and Molinari 2003) on the second stage of the rainfall,

Though FNL has a resolution of about 100 km, its vertical velocity is reliable because of a good consistency

between the vertical velocity (thin contours in Fig. 9) and the 6-h accumulated rainfall ± 3 h relative to different times in the second stage (shaded in Fig. 9). The most intense rainfall at this stage is mostly 400 km away from the center and on the downshear side of the TC circulation with an apparent preference of the downshear-right quadrant. This rainfall pattern is consistent with observational studies that demonstrated that the rainfall associated with a weak system or in the outer rainbands has a preference of location on the downshear or downshear right (Corbosiero and Molinari 2002, 2003; Cecil 2007).

This downshear-right preference may be interpreted by the vortex-tilting mechanism (Jones 1995). To be specific, in an adiabatic situation, vertical shear tends to tilt the vortex toward downshear. Then adiabatic lifting

occurs to produce a cold anomaly in balance with the tilted positive PV anomaly. The adiabatic cooling in down-tilt ascending air and warming in up-tilt descending air distorts the isentropes. The deformed isentropes are higher on down tilt than on up tilt. The cyclonic flow of the vortex moves along the slopes of the distorted isentropes adiabatically and thus results in upward motion on the right side of the tilting vector and downward motion on the left side of the tilting vector facing down tilt. As a result, rainfall will appear on the right side of the tilting vector. The rainfall could be farther advected to down tilt or down tilt left by the cyclonic circulation of the vortex. The stronger the vortex is, the farther to the down-tilt left the rainfall will be advected.

For a loosely organized cyclone or outer rainbands, the vortex has a large expanse of unsaturated air, and therefore the vortex-tilting mechanism, which works under adiabatic conditions, could be used to explain the rainfall on down-tilt right and down tilt in a weak cyclone or in outer rainbands, which is just what we are examining in the Bilis case. After making landfall, Bilis quickly weakened and the heavy rainfall appeared largely 400 km away from the cyclone center. The tilting vector, which was determined by the vector pointing from the circulation center at 850 hPa toward the one at 300 hPa, is also plotted in Fig. 9 (marked by "T"). Except for 1800 UTC 14 July 2006, the tilting vectors at the three other times are close to the shear vectors. It is apparent that the vertical motion and the associated rainfall are mainly located on down tilt or down-tilt right.

The applicability of the vortex-tilting mechanism becomes questionable under diabatic conditions because latent heating from convection will likely cancel the corresponding adiabatic cooling. One possible mechanism for the downshear upward motion in this situation is the relative flow mechanism or vorticity balance argument (Willoughby 1984; Wang and Holland 1996; Bender 1997; Frank and Ritchie 2001; Braun et al. 2006; Wu et al. 2006). To be specific, in a unidirectional shear environment, if the cyclone moves with the ambient flow at a certain level, the relative flow will blow inward at low levels and outward at upper levels on the downshear side. Then negative vorticity advection will appear at low levels and positive vorticity advection will appear at

upper levels. Because of the vorticity conservation constraint, the negative (positive) vorticity advection will be balanced by vortex stretching (shrinking). As a result, low-level convergence and upper-level divergence and a deep layer of upward motion on the downshear side of the vortex will appear. The opposite occurs on the upshear side.

To explore the possibility of the relative flow mechanism in our case, we calculated asymmetric flow by subtracting out the azimuthally averaged tangential and radial velocity from the total wind similar to Braun et al. (2006). The asymmetric flow is northward or northeastward at 850 hPa and westward or southwestward at 300 hPa (Fig. 10). Negative vorticity advection associated with low-level inflow and positive vorticity advection associated with upper-level outflow observed on the downshear side are consistent with low-level convergence and upper-level divergence (shaded in Fig. 10) and a deep layer of vertical motion (dotted contours in Fig. 10) on the downshear side. As a consequence, the relative flow mechanism could be valid at least qualitatively in interpreting the impact of vertical wind shear on the observed vertical motion on the downshear side. This result complements Braun et al. (2006), which focuses on the eyewall vertical motion.

The impact of vertical wind shear on the vertical motion not only can be examined from the aspect of vortex–shear interaction as described in this section, but also can be analyzed from warm-air advection through quasigeostrophic (QG) forcing.

c. Warm-air advection

The QG omega equation has been widely used to diagnose synoptic vertical motion (Sutcliffe 1947; Hoskins et al. 1978; Trenberth 1978; Durran and Snellman 1987; Raisanen 1995). It indicates the vertical motion induced by geostrophic advection of temperature and vorticity. In essence, vertical motion due to geostrophic forcing is a result of the atmosphere's restoring of thermal wind balance disrupted by geostrophic advection. Raisanen (1995) diagnosed vertical motion forcing in a global domain using a spectral truncation of T63 with the QG omega equation. He found that the average correlation between QG and generalized vertical motion is nearly 0.6 in the subtropics (15°–30°N). The standard form of the QG omega equation is as follows:

$$\left(\sigma \nabla^2 + f_0^2 \frac{\partial^2}{\partial p^2} \right) \omega = f_0 \frac{\partial}{\partial p} \left[\underbrace{\mathbf{V}_g \cdot \nabla \left(\frac{1}{f_0} \nabla^2 \Phi + f \right)}_{F_V} \right] + \nabla^2 \left[\underbrace{\mathbf{V}_g \cdot \nabla \left(-\frac{\partial \Phi}{\partial p} \right)}_{F_T} \right]. \quad (1)$$

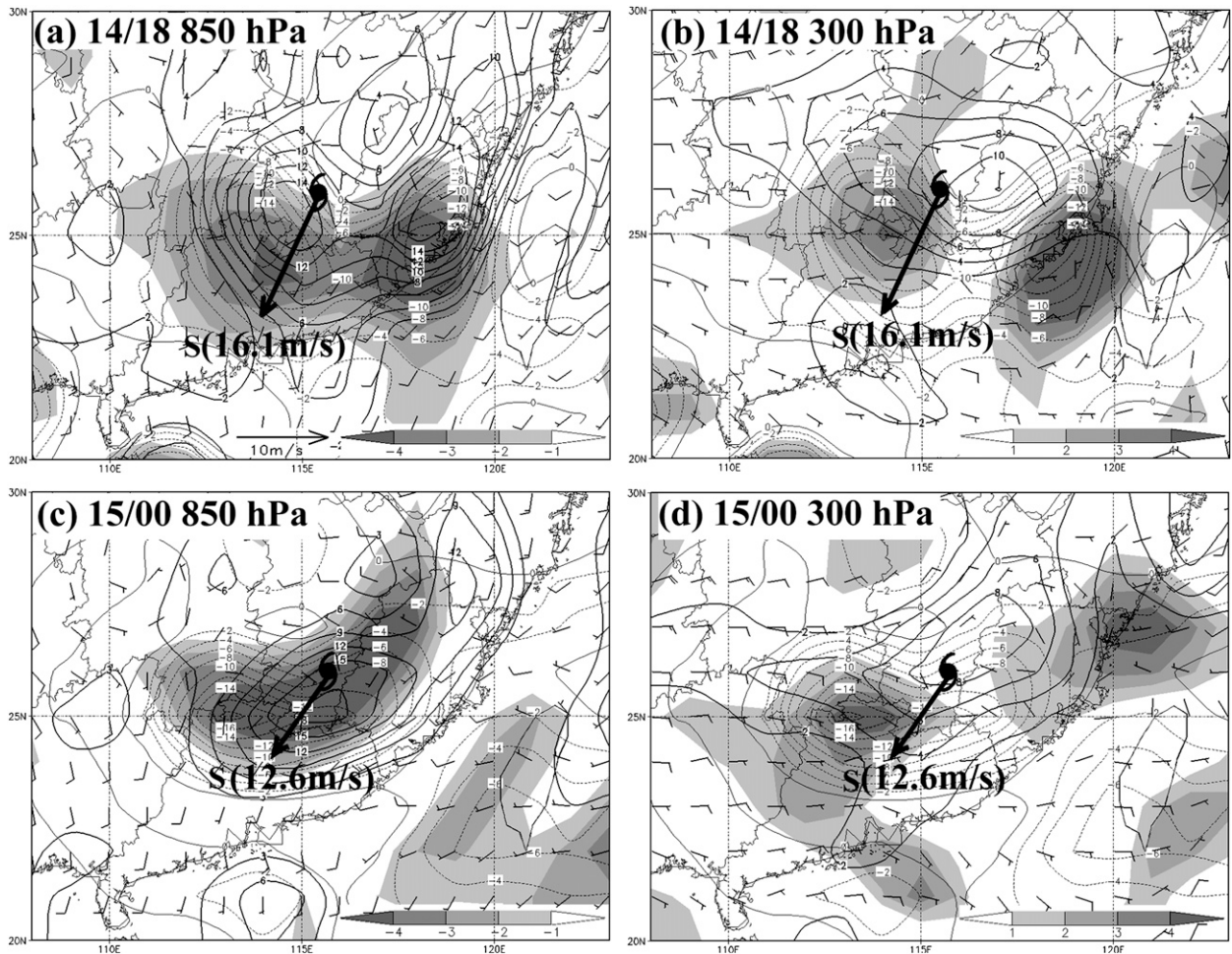


FIG. 10. The asymmetric winds (full barb = 10 m s^{-1}) and relative vertical vorticity (solid contours; 10^{-5} s^{-1}) at (a) 1800 UTC 14 Jul 2006 at 850 hPa, (b) 1800 UTC 14 Jul 2006 at 300 hPa, (c) 0000 UTC 15 Jul 2006 at 850 hPa, and (d) 0000 UTC 15 Jul 2006 at 300 hPa. The convergence at 850 hPa, divergence at 300 hPa (shaded; 10^{-5} s^{-1}), upward velocity at 700 hPa (dotted contour; $10^{-1} \text{ Pa s}^{-1}$), and vertical wind shear vector (black arrow denoted by “S” with its magnitude) between 200 and 850 hPa are also plotted for reference. The typhoon symbol denotes the circulation center of Bilis in the FNL analysis at 850 hPa at the corresponding times.

The first term on the right-hand side (F_V) represents differential vorticity advection. The second term on the right-hand side (F_T) represents Laplacian of thermal advection. Because we are interested in the possible mechanism of vertical motion, we only calculated the forcing on the right-hand side instead of solving the whole equation. We also calculated the divergence of the quasigeostrophic \mathbf{Q} vector, which is generally similar to but more accurate than $F_V + F_T$. We chose to use the standard form of the omega equation to evaluate the relative importance of the differential absolute vorticity advection and Laplacian of thermal advection.

The total forcing at 700 hPa is generally consistent with the upward motion (Fig. 11) though their maximum centers somewhat deviate from each other because of other possible lifting mechanisms such as oro-

graphic lifting. This result indicates that synoptic forcing through quasigeostrophic dynamics could have contributed to the rainfall.

The relative dominance of geostrophic vorticity and thermal advection is examined by calculating the difference between the absolute values of F_V and F_T : $|F_V| - |F_T|$ (heavy contours in Fig. 11). Positive (negative) values of $|F_V| - |F_T|$ mean that F_V (F_T) is the dominating factor. The result shows that the QG vertical motions in northern Guangdong at 1200 UTC 14 July and in southern Hunan at 0000 and 0006 UTC 15 July are mainly produced by geostrophic vorticity advection. The geostrophic vertical motion in southern Guangdong at 1200 UTC 14 July, most parts of Guangdong at 0000 and 0006 UTC 15 July, and border regions between Hunan, Guangdong, and Guangxi at 1800 UTC 14 July

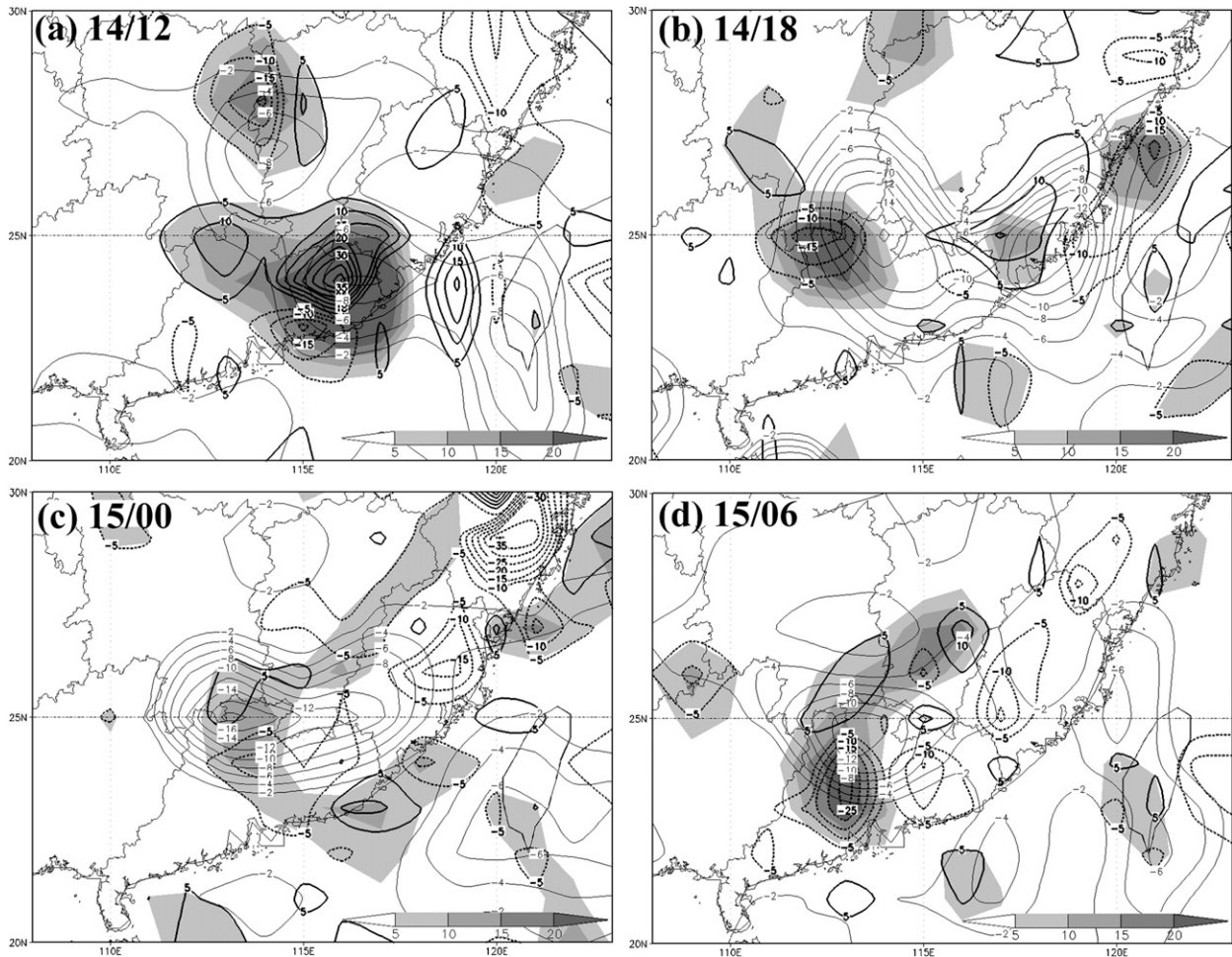


FIG. 11. The QG forcing for upward motion by summing the two terms on the right-hand side of the QG omega equation (shaded every $5 \times 10^{-18} \text{ m kg}^{-1} \text{ s}^{-1}$; only positive value are plotted), the relative importance of F_V and F_T (heavy contour: solid for dominance of F_V and dashed for dominance of F_T), and upward velocity (thin contour; $10^{-1} \text{ Pa s}^{-1}$) at 700 hPa at (a) 1200 UTC 14 Jul, (b) 1800 UTC 14 Jul, (c) 0000 UTC 15 Jul, and (d) 0600 UTC 15 Jul 2006.

2006 are largely due to thermal advection. This result suggests that warm-air advection could have played an important role in producing the vertical motion through geostrophic advection of temperature. The dominance of F_T is consistent with low-level warm-air advection indicated by the veering winds of radiosondes at Ganzhou (Jiangxi Province), Chenzhou (Hunan Province), and Qingyuan (Guangdong Province) (Fig. 4).

d. Frontogenesis

Petterssen (1936) defined atmospheric frontogenesis as the Lagrangian rate of change of the magnitude of horizontal potential temperature gradient due to horizontal wind. Through driving an ageostrophic direct circulation, Petterssen frontogenesis is useful in diagnosing vertical motion and has been shown to be a good predictor for rainfall (Harr et al. 2000; Harr and Elsberry

2000; Colle 2003). Following Schultz and Doswell (1999), the Petterssen form of frontogenesis can be expressed as:

$$F = \frac{d}{dt} |\nabla_h \theta| = \frac{-1}{|\nabla_h \theta|} \left\{ \left[\left(\frac{\partial \theta}{\partial x} \right)^2 \left(\frac{\partial u}{\partial x} \right) + \left(\frac{\partial \theta}{\partial y} \right)^2 \left(\frac{\partial v}{\partial x} \right) \right] + \left[\frac{\partial \theta}{\partial x} \frac{\partial \theta}{\partial y} \left(\frac{\partial v}{\partial x} + \frac{\partial u}{\partial y} \right) \right] \right\}. \quad (2)$$

In (2), θ denotes potential temperature, and u and v represent horizontal wind components in Cartesian coordinates. Figure 12 shows that the convergence well collocates with confluence at 850 hPa, producing substantial frontogenesis at different times in the area of strong vertical motion, suggesting that frontogenesis could have played an important role in forcing the vertical motion. On the other hand, the impact of differential solar heating of land surface on the frontogenesis

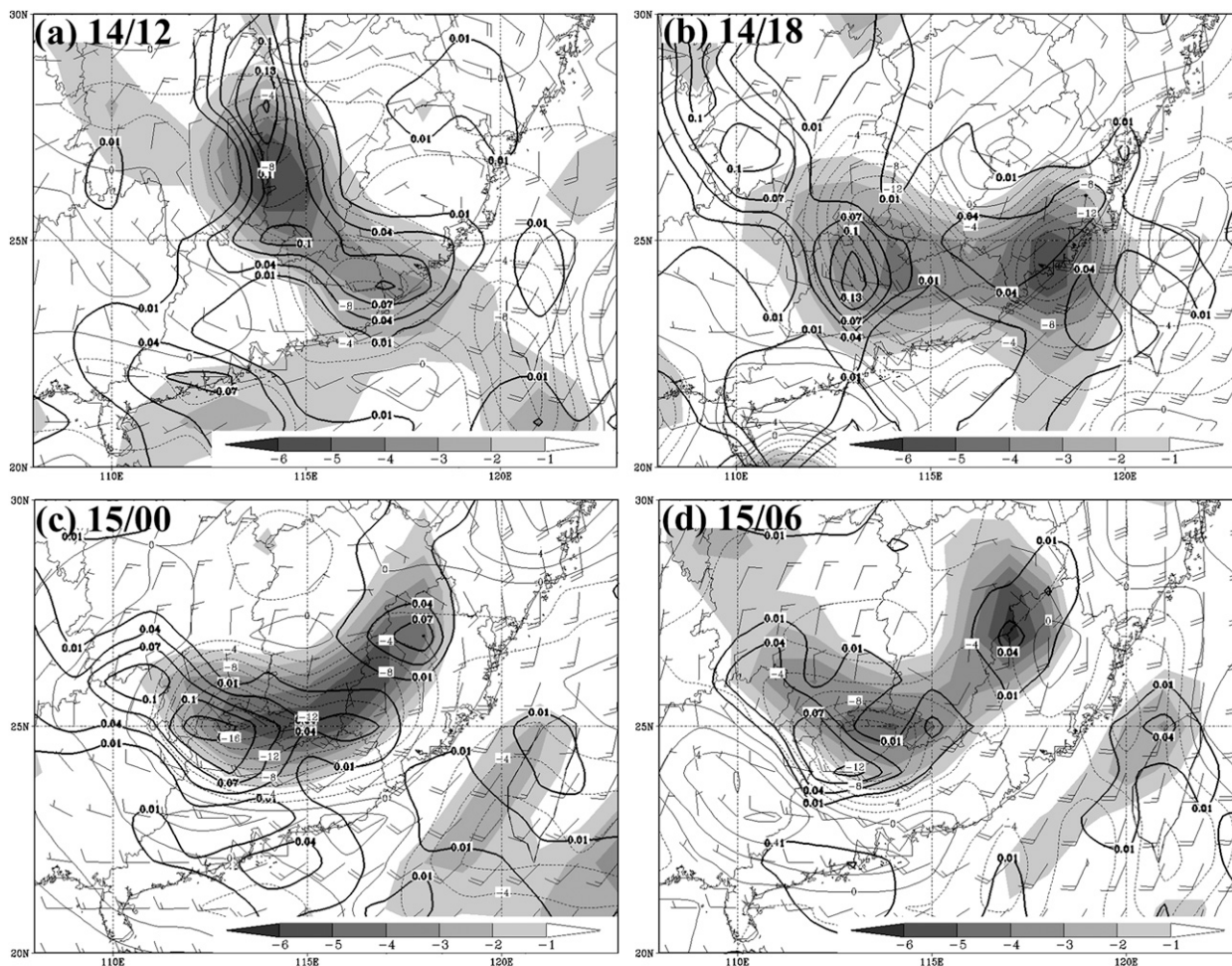


FIG. 12. The frontogenesis ($10^{-2} \text{ K km}^{-1} \text{ h}^{-1}$; solid), convergence (shaded; 10^{-5} s^{-1}), and wind vector (full barb = 10 m s^{-1}) at 850 hPa at (a) 1200 UTC 14 Jul, (b) 1800 UTC 14 Jul, (c) 0000 UTC 15 Jul, and (d) 0600 UTC 15 Jul 2006. The vertical velocities (thin contour; $10^{-1} \text{ Pa s}^{-1}$) at 700 hPa at the respective times are also plotted.

is likely to be minor in our case because of the continuous rainfall during the entire second stage.

Overall, the above analyses indicate that an overlapping of all three ingredients of deep moist convection is observed during the second stage of rainfall. Lifting necessary to produce rainfall during the second stage could be contributed by interaction of the vertical wind shear with the TC vortex, warm-air advection, frontogenesis, and topography. Because all of these processes are present, it is hard to pinpoint which of them is the single most important contributor for the current observational study. It is possible that all of these factors, which are dynamically interrelated, are necessary for this record-breaking flooding event.

6. Summary and discussion

Using the real-time observational data archive from CNMC and the FNL global gridded analysis from NCEP,

this study explores possible mechanisms of torrential rainfalls over large areas of southern China induced by Bilis, a western North Pacific severe tropical storm that made landfall on the southeastern coast of mainland China on 14 July 2006 and persisted over land until after 17 July 2006.

From the observational analyses, it is found that the heavy rainfall associated with Bilis can be roughly divided into three stages based on the timing and location. The first stage of the rainfall happened in Fujian and Zhejiang Provinces and could be directly induced by the inner-core circulation during Bilis's landfall. The second stage of rainfall caused the most catastrophic flooding and is the primary focus of the current study. It occurred inland near the border regions between Jiangxi, Hunan, and Guangdong Provinces. This stage of the rainfall could be attributed to moist and unstable flow along with lifting from vortex–shear interaction, warm-air

advection, frontogenesis, and topography. The third stage of rainfall that occurred along the coastal areas of Guangdong and Fujian Provinces likely resulted from the interaction of Bilis circulation with the South China Sea monsoon enhanced by topographical lifting along the coast.

The mechanism of the second stage of rainfall was explored using an ingredients-based method. The result shows that the rainfall could be a result of all three ingredients of deep moist convection (moisture, instability, and lifting) getting together. Possible lifting mechanisms associated with the rainfall in the second stage were investigated in detail. Strong vertical shear is observed in this stage of rainfall. The rainfall is mainly located on the downshear side of Bilis with a preference on down-tilt and downshear right. This is consistent with previous observational studies (Corbosiero and Molinari 2002, 2003; Lonfat et al. 2004; Cecil 2007). Impact of vertical shear on rainfall distribution may come from vortex tilting and the vorticity balance argument. Consistent with the vertical wind shear, widespread low-level warm-air advection is found in southeastern China, which may also contribute to low-level lifting through quasigeostrophic forcing. Furthermore, the low-level convergence together with flow (confluence) deformation produces significant frontogenesis that collocates well with the observed vertical motion and associated rainfall. Through numerical sensitivity experiments using WRF with and without the complex topography, it is found that the influence of complex topography is secondary for the second stage of the rainfall, despite some apparent local enhancement and redistribution of precipitation.

Since diagnosis of the omega equation, vertical shear, vortex tilting, and frontogenesis can be easily applied to any gridded observational analysis or forecast field in real time, they may be used as a guidance to forecast heavy rainfall events associated with TCs after they move inland. It is worth cautioning the generality of this single case to other landfalling TCs. In particular, our results are obviously limited by the quality and the resolution of the NCEP global analysis.

Acknowledgments. The authors are grateful to Dalin Zhang and Jason Sippel for helpful discussions and comments on this subject and to Liu Zhengkun for data and technical help. Formal review comments by David Schultz and three other anonymous reviewers are also acknowledged. This research is sponsored by the Office of Navy Research under Grant N000140410471, China National Basic Research Program under Grant 2004CB418307, National Science Foundation of China under Grant 40730948, and the China National Meteorological Center.

REFERENCES

- Atallah, E., and L. F. Bosart, 2003: Extratropical transition and precipitation distribution: A case study of Floyd (1999). *Mon. Wea. Rev.*, **131**, 1063–1081.
- , —, and A. R. Aiyyer, 2007: Precipitation distribution associated with landfalling tropical cyclones over the eastern United States. *Mon. Wea. Rev.*, **135**, 2185–2206.
- Bender, M. A., 1997: The effect of relative flow on the asymmetric structure in the interior of hurricanes. *J. Atmos. Sci.*, **54**, 703–724.
- Beven, J. L., II, and J. Franklin, 2004: Eastern North Pacific hurricane season of 1999. *Mon. Wea. Rev.*, **132**, 1036–1047.
- Braun, S. A., and L. Wu, 2007: A Numerical study of Hurricane Erin (2001). Part II: Shear and the organization of eyewall vertical motion. *Mon. Wea. Rev.*, **135**, 1179–1194.
- , M. T. Montgomery, and Z. Pu, 2006: High-resolution simulation of Hurricane Bonnie (1998). Part I: The organization of eyewall vertical motion. *J. Atmos. Sci.*, **63**, 19–42.
- Cecil, D. J., 2007: Satellite-derived rain rates in vertically sheared tropical cyclones. *Geophys. Res. Lett.*, **34**, L02811, doi:10.1029/2006GL027942.
- Chen, S., J. A. Knaff, and F. D. Marks Jr., 2006: Effects of vertical wind shear and storm motion on tropical cyclone rainfall asymmetries deduced from TRMM. *Mon. Wea. Rev.*, **134**, 3190–3208.
- China Meteorological Administration, 2007: *Yearbook of Meteorological Disasters (2007)*, X. Xu, Ed., Meteorological Press of China, 260 pp.
- Cline, I. M., 1926: *Tropical Cyclones*. MacMillan, 301 pp.
- Colle, B. A., 2003: Numerical simulation of the extratropical transition of Floyd (1999): Structural evolution and responsible mechanisms for the heavy rainfall over the northeast United States. *Mon. Wea. Rev.*, **131**, 2905–2926.
- Corbosiero, K. L., and J. Molinari, 2002: The effects of vertical wind shear on the distribution of convection in tropical cyclones. *Mon. Wea. Rev.*, **130**, 2110–2123.
- , and —, 2003: The relationship between storm motion, vertical wind shear, and convective asymmetries in tropical cyclones. *J. Atmos. Sci.*, **60**, 366–376.
- Doswell, C. A., III, H. E. Brooks, and R. A. Maddox, 1996: Flash flood forecasting: An ingredients-based methodology. *Wea. Forecasting*, **11**, 560–581.
- Duan, Y., 2006: Typhoons Bilis and Saomai: Why the impacts were so severe. *WMO Bull.*, **55** (4), 280–284.
- Dunn, G. E., and B. I. Miller, 1960: *Atlantic Hurricanes*. Louisiana State University Press, 377 pp.
- Durran, D. R., and L. W. Snellman, 1987: The diagnosis of synoptic-scale vertical motion in an operational environment. *Wea. Forecasting*, **2**, 17–31.
- Frank, W. M., and E. A. Ritchie, 1999: Effects of environmental flow upon tropical cyclone structure. *Mon. Wea. Rev.*, **127**, 2044–2061.
- , and —, 2001: Effects of vertical wind shear on the intensity and structure of numerically simulated hurricanes. *Mon. Wea. Rev.*, **129**, 2249–2269.
- Grell, G. A., and D. Devenyi, 2002: A generalized approach to parameterizing convection combining ensemble and data assimilation techniques. *Geophys. Res. Lett.*, **29**, 1693, doi:10.1029/2002GL015311.
- Harr, P. A., and R. L. Elsberry, 2000: Extratropical transition of tropical cyclones over the western North Pacific. Part I:

- Evolution of structural characteristics during the transition process. *Mon. Wea. Rev.*, **128**, 2613–2633.
- , —, and T. F. Hogan, 2000: Extratropical transition of tropical cyclones over the Western North Pacific. Part II: The impact of midlatitude circulation characteristics. *Mon. Wea. Rev.*, **128**, 2634–2653.
- Hong, S.-Y., J. Dudhia, and S.-H. Chen, 2004: A revised approach to ice microphysical processes for the parameterization of clouds and precipitation. *Mon. Wea. Rev.*, **132**, 103–120.
- Hoskins, B. J., I. Draghici, and H. C. Davies, 1978: A new look at the ω equation. *Quart. J. Roy. Meteor. Soc.*, **104**, 31–38.
- Houze, R. A., S. S. Chen Jr., B. F. Smull, W.-C. Lee, and M. M. Bell, 2007: Hurricane intensity and eyewall replacement. *Science*, **315**, 1235–1239.
- Jones, R. W., 1987: A simulation of hurricane landfall with a numerical model featuring latent heating by the resolvable scales. *Mon. Wea. Rev.*, **115**, 2279–2297.
- Jones, S. C., 1995: The evolution of vortices in vertical shear: Initially barotropic vortices. *Quart. J. Roy. Meteor. Soc.*, **121**, 821–851.
- , 2000a: The evolution of vortices in vertical shear. II: Large-scale asymmetries. *Quart. J. Roy. Meteor. Soc.*, **126**, 3137–3159.
- , 2000b: The evolution of vortices in vertical shear. III: Baroclinic vortices. *Quart. J. Roy. Meteor. Soc.*, **126**, 3161–3185.
- Li, J., and Coauthors, 2003: Advancement in the study of typhoon rainstorm (in Chinese). *J. Trop. Meteor.*, **19** (Suppl.), 152–159.
- , A. Y. Wany, E. B. Hou, G. L. Li, X. J. He, T. Y. Peng, and Q. Zeng, 2004: A numerical prediction experiment of track and heavy rainfall round about Typhoon Fitow. *J. Trop. Oceanogr.*, **23**, 16–24.
- Lin, Y. L., S. Chiao, T.-A. Wang, M. L. Kaplan, and R. P. Weglarz, 2001a: Some common ingredients of heavy orographic rainfall. *Wea. Forecasting*, **16**, 633–660.
- Lin, Y. Y., Y. Q. Liu, and L. Q. Zhang, 2001b: An analysis on the impact of Severe Tropical Storm “Maria” on the torrential heavy rain in Shaoguan. *Guangdong Meteor.*, **3**, 5–7.
- Lonfat, M., and F. D. Marks Jr., Chen, S. S., 2004: Precipitation distribution in tropical cyclones using the Tropical Rainfall Measuring Mission (TRMM) Microwave Imager: A global perspective. *Mon. Wea. Rev.*, **132**, 1645–1660.
- Miller, B. L., 1964: A study of the filling of Hurricane Donna (1960) over land. *Mon. Wea. Rev.*, **92**, 389–406.
- Noh, Y., W.-G. Cheon, S.-Y. Hong, and S. Raasch, 2003: Improvement of the K-profile model for the planetary boundary layer based on large eddy simulation data. *Bound.-Layer Meteor.*, **107**, 401–427.
- Pasch, R. J., M. B. Lawrence, L. A. Avila, J. L. Beven, J. L. Franklin, and S. R. Stewart, 2004: Atlantic hurricane season of 2002. *Mon. Wea. Rev.*, **132**, 1829–1859.
- Petterssen, S., 1936: Contribution to the theory of frontogenesis. *Geophys. Publ.*, **11** (6), 27 pp.
- Powell, M. D., 1987: Changes in the low-level kinematic and thermodynamic structure of Hurricane Alicia (1983) at landfall. *Mon. Wea. Rev.*, **115**, 75–99.
- Raisanen, J., 1995: Factors affecting synoptic-scale vertical motions: A statistical study using a generalized omega equation. *Mon. Wea. Rev.*, **123**, 2447–2460.
- Rappaport, E. N., 2000: Loss of life in the United States associated with recent Atlantic tropical cyclones. *Bull. Amer. Meteor. Soc.*, **81**, 2065–2073.
- Rogers, R., S. Chen, and J. Tenerelli, 2003: A numerical study of the impact of vertical shear on the distribution of rainfall in Hurricane Bonnie (1998). *Mon. Wea. Rev.*, **131**, 1577–1599.
- Schultz, M. D., and C. A. Doswell, 1999: Conceptual models of upper-level frontogenesis in south-westerly and north-westerly flow. *Quart. J. Roy. Meteor. Soc.*, **125**, 2535–2562.
- Shapiro, L. J., 1983: Asymmetric boundary layer flow under a translating hurricane. *J. Atmos. Sci.*, **40**, 1984–1998.
- Sutcliffe, R. C., 1947: A contribution to the problem of development. *Quart. J. Roy. Meteor. Soc.*, **73**, 370–383.
- Trenberth, K. E., 1978: On the interpretation of the diagnostic quasi-geostrophic omega equation. *Mon. Wea. Rev.*, **106**, 131–137.
- Tuleya, R. E., and Y. Kurihara, 1978: A numerical simulation of the landfall of tropical cyclones. *J. Atmos. Sci.*, **35**, 242–257.
- Wang, Y., and G. J. Holland, 1996: Tropical cyclone motion and evolution in vertical shear. *J. Atmos. Sci.*, **53**, 3313–3332.
- Willoughby, H. E., and F. D. Marks, Feinberg, R. J., Jr., 1984: Stationary and moving convective bands in hurricanes. *J. Atmos. Sci.*, **41**, 3189–3211.
- Wu, L. G., S. A. Braun, J. Halverson, and G. Heymefield, 2006: A numerical study of Hurricane Erin (2001). Part I: Model verification and storm evolution. *J. Atmos. Sci.*, **63**, 65–86.
- Zhao, Y., Z. Wu, S. Liu, and D. Gong, 2005: Potential vorticity analysis of a torrential rain triggered by a neutercane in Shandong province (in Chinese). *J. Trop. Meteor.*, **21**, 32–43.